Max deletion destabilizes MYC protein and abrogates Eμ-*Myc* lymphomagenesis

Haritha Mathsyaraja, Brian Freie, Pei-Feng Cheng, Ekaterina Babaeva, Jonathen T. Catchpole, Derek Janssens, Steven Henikoff, and Robert N. Eisenman

Basic Sciences Division, Fred Hutchinson Cancer Research Center, Seattle, Washington 98109, USA

Although MAX is regarded as an obligate dimerization partner for MYC, its function in normal development and neoplasia is poorly defined. We show that B-cell-specific deletion of *Max* has a modest effect on B-cell development but completely abrogates Eμ-*Myc*-driven lymphomagenesis. While *Max* loss affects only a few hundred genes in normal B cells, it leads to the global down-regulation of *Myc*-activated genes in premalignant Eμ-*Myc* cells. We show that the balance between MYC–MAX and MNT–MAX interactions in B cells shifts in premalignant B cells toward a MYC-driven transcriptional program. Moreover, we found that MAX loss leads to a significant reduction in MYC protein levels and down-regulation of direct transcriptional targets, including regulators of MYC stability. This phenomenon is also observed in multiple cell lines treated with MYC–MAX dimerization inhibitors. Our work uncovers a layer of *Myc* autoregulation critical for lymphomagenesis yet partly dispensable for normal development.

[*Keywords*: B-cell development; MAX; MYC stability; lymphomagenesis; transcription]

Supplemental material is available for this article.

Received February 22, 2019; revised version accepted June 14, 2019.

The MAX protein was first identified as a specific dimerization partner with members of the MYC oncoprotein family (MYC, MYCN, and MYCL). Like MYC, MAX is a member of the basic region helix–loop–helix zipper (bHLHZ) class of transcriptional regulators, and the association of MYC with MAX is mediated by heterodimerization between their two HLHZ domains. MYC–MAX heterodimers bind DNA through direct contact of each bHLHZ basic region with the major groove of E-box DNA sequences (CANNTG) (for reviews, see Conacci-Sorrell et al. 2014; Carroll et al. 2018). MYC does not homodimerize or bind DNA under physiological conditions and, aside from MAX, no other bHLHZ proteins have been compellingly demonstrated to dimerize with MYC. Because mutations in the MYC bHLHZ that prevent association with MAX also block MYC's major biological activities, it has been generally assumed that MAX is required for MYC function. Indeed, studies in the 1990s demonstrated that heterodimerization with MAX is required for MYC's DNA-binding and transcriptional activities as well as for cell transformation (Blackwood and Eisenman 1991; Blackwood et al. 1992; Kretzner et al. 1992; Amati et al. 1993). Moreover, targeted deletion of *Max* in mice results in early postimplantation lethality, consistent with essential functions for *Myc* and *MycN* during embryonic development (Shen-li et al. 2000). In addition to dimerizing with MYC family proteins, MAX also forms E-box DNA-binding heterodimers with the MXD family and MNT and MGA proteins, all of which act as transcriptional repressors.

Despite the apparent centrality of MAX for the functions of multiple bHLHZ transcription factors, there is evidence that MAX loss of function can be tolerated and even oncogenic in several biological contexts. For example, pheochromocytoma cell lines can proliferate in the absence of MAX, and a subset of familial pheochromocytomas is strongly associated with inactivation of MAX (Hopewell and Ziff 1995; Comino-Méndez et al. 2011). In addition, ~6% of human small cell lung carcinomas (SCLC) exhibit loss of MAX, and introduction of MAX into human SCLC lines lacking MAX arrests growth (Romero et al. 2014). Last, in *Drosophila melanogaster*, larval development is less compromised by loss of MAX than by loss of MYC, and several critical activities of MYC appear unaffected by MAX inactivation (Steiger et al. 2008). These findings suggest that there are functions of MYC independent of MAX and that loss of MAX in some settings can promote oncogenic conversion.

To investigate a MAX-independent role in MYC-induced oncogenesis, we turned to Eμ-*Myc* transgenic mice, which model the 8;14 translocation found in Burkitt's B-cell lymphomas and have provided many insights

Corresponding author: eisenman@fhcrc.org
Article published online ahead of print. Article and publication date are online at http://www.genesdev.org/cgi/doi/10.1101/gad.325878.119.

into MYC-driven lymphomagenesis. The overexpression of MYC produces a polyclonal increase in pre-B cells in young mice, accompanied by reduced differentiation to mature B cells (Harris et al. 1988). Earlier work using an Eμ-*Max* transgene established that overexpression of MAX alone in murine lymphoid cells is nononcogenic and results in reduced B-cell proliferation and numbers. Importantly, in the context of an Eμ-*Myc* transgene, augmented expression of *Max* also attenuated B-cell lymphomagenesis and reduced lymphoproliferation (Lindeman et al. 1995), indicating that the ratio of MYC:MAX expression levels can influence MYC function. However, the requirement for endogenous MAX in MYC-induced tumorigenesis has not been determined. To address these questions, we generated a conditional *Max* allele to elucidate *Max* function in lymphomagenesis and in B-cell homeostasis.

Results

Max *deletion partially impairs B-cell development*

We constructed a *Max* targeting vector by inserting *loxP* sites flanking exon 4 within a full-length *Max* genomic clone. This region encodes nearly the entire helix 2 leucine zipper region of *Max* necessary for dimerization with MYC and other bHLHZ proteins (Fig. 1A), and its Cre-mediated deletion results in a frameshift and truncation within exon 5, leading to a 127-amino-acid protein lacking the HLHZ domain. Expression of Cre in $Max^{fl/+}$ embryonic stem (ES) cells resulted in heterozygous deletion of *Max* ($Max^{\Delta/+}$), and these ES cells were used to produce chimeric mice. Extensive intercrossing of $Max^{\Delta/+}$ F1 mice failed to produce any homozygous *Max*-null offspring, consistent with a previous report (Supplemental Fig. S1A; Shen-li et al. 2000).

We next crossed $Max^{fl/fl}$ mice with hemizygous $Max^{fl/fl}$ mb1-Cre transgenic mice. Expression of the mb1 gene is restricted to B cells beginning at the early pro-B-cell stage, and mb1-Cre and has been used extensively to study B-cell development and function (Hobeika et al. 2006). MAX protein was detected in $B220^+$ splenocytes in $Max^{fl/fl}$ mice (referred to here as *Max* WT [wild type]) using an antibody against the C terminus, while mb1-Cre; $Max^{fl/fl}$ cells (referred to as *Max* knockout) did not express any protein reactive with the antibody (Fig. 1B).

We examined the consequences of *Max* deletion on normal B-cell development by comparing *Max* WT with *Max* knockout mice. Using flow cytometry to assess cell subpopulations in the B-cell lineage (Supplemental Fig. S1B), we noted a significant decrease in the numbers of B220-positive, IgM^-, and IgM^+ B cells from Max knockout relative to WT (Fig. 1C). Notably, $B220^+$ IgM^+ B cells (pre-B cells) were nearly 10-fold lower in *Max* knockout samples than in *Max* WT (Fig. 1D; Supplemental Table S1). More detailed analysis of different stages of B-cell development showed that while the proportions of prepro-B and pro-B cells were approximately the same in mice of the two genotypes, the percentage of pre-B, immature B, and mature B cells was strikingly diminished in *Max* knockout mice, indicating that loss of *Max* results in a significant block in pro-B-to-pre-B-cell differentiation (Fig. 1D; Supplemental Table S1). This block in development is similar to that seen upon *Myc* loss in B cells (Habib et al. 2007). In

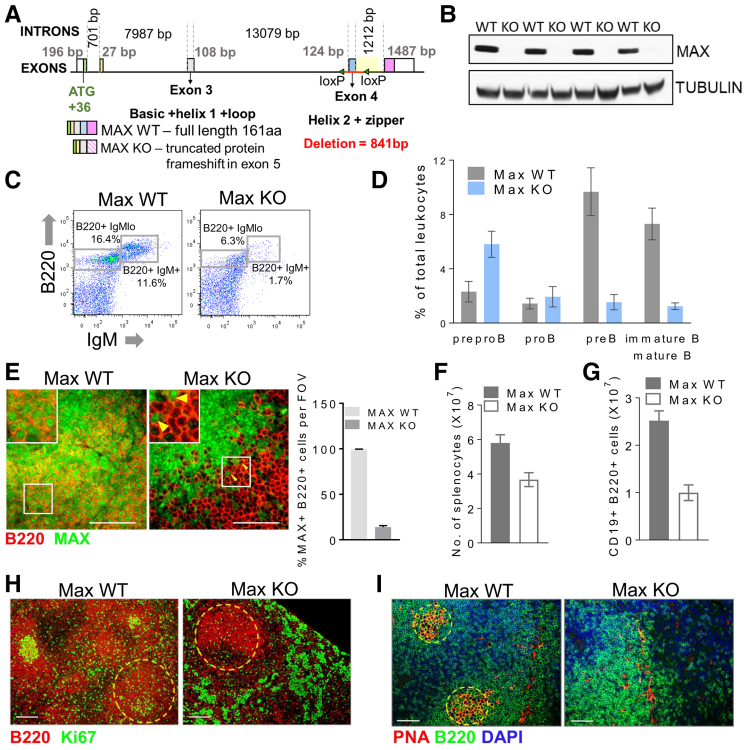

Figure 1. Conditional deletion of Max in the B-cell lineage. (*A*) Schematic depicting the location of loxP sites at the *Max* locus. (*B*) Representative immunoblots for MAX in $B220^+$ splenocytes from $Max^{fl/fl}$ (wild-type [WT]) and $Max^{fl/fl}$ mb1-cre (knockout [KO]) animals. (*C*) Representative flow plots showing $B220^+$ and IgM^+ populations in CD45 gated bone marrow (BM) cells. (*D*) Quantification of B lymphocyte precursor populations in Max WT ($n = 5$) and knockout ($n = 6$) BM. (*E*) Dual immunofluorescence (IF) for MAX and B220 in spleens. Quantification of MAX^+ $B220^+$ cells from MAX knockout spleens. $n = 3$. Yellow arrowheads indicate MAX^+ $B220^+$ cells in *Max* knockout. Total number of splenocytes (*F*) and $CD19^+$ $B220^+$ cells (*G*) in Max WT and knockout mice. WT $n = 8$; knockout $n = 9$. (*H*) IF staining for B220 and proliferation marker Ki67 in *Max* WT and knockout spleens. (*I*) IF staining of germinal centers (PNA) in *Max* WT and knockout spleens. Representative image. $n = 3$ animals per genotype. Scale bars, 100 μM. All error bars represent SEM.

addition, bone marrow (BM) precursors from *Max* knockout mice failed to efficiently differentiate into B220$^+$ cells upon treatment with IL-7 in vitro (Supplemental Fig. S1C, D). We also noted a compensatory increase in the percentages of CD3$^+$ T cells and CD11b$^+$ myeloid cells (Supplemental Fig. S1E). To study mature B-cell populations, we examined spleens of *Max* knockout mice. A majority (~86%) of B220$^+$ cells lacked detectable MAX staining in their nuclei (Fig. 1E), accompanied by reduced numbers of total (Fig. 1F) and CD19$^+$ B220$^+$ splenocytes in *Max* knockout spleens (Fig. 1G; Supplemental Fig. S1F). Indeed, B220$^+$ areas in the spleen displayed reduced Ki67 staining, especially in regions corresponding to germinal centers (GCs) (Fig. 1H; Supplemental Fig. S1G). Since MYC is known to play a critical role in GC formation and maintenance (Calado et al. 2012), we stained spleens for PNA, a GC B-cell marker. Although nonimmunized mice have relatively few GCs, we still observed positive staining for PNA in *Max* WT mice, which was absent in *Max* knockout spleens (Fig. 1I), suggesting that MAX plays a critical role in GC formation. Our results suggest that *Max* is not essential for B lymphocyte development and differentiation. Of note, our data on BM development, splenic B-cell numbers, and GC phenotypes are largely consistent with a recent study from the de Alboran laboratory (Pérez-Olivares et al. 2018) using CD19-cre to delete *Max*.

We also found that depletion of *Max* in the T-cell lineage using lck-cre led to marginally impaired differentiation of double-negative (DN) to double-positive (DP) thymocytes (Supplemental Fig. S1H). Taken together, our data indicate that *Max* loss attenuates overall lymphocyte development rather than completely abolishing it.

Requirement for Max *in activated lymphocytes and Eμ-*Myc*-induced lymphomagenesis*

To study the requirement for *Max* in situations where *Myc* expression is elevated, we activated B220$^+$ B cells in vitro using bacterial lipopolysaccharides (LPSs). We found activation to be severely compromised in *Max* knockout mice, and B cells exhibited little increase in cell size (Fig. 2A). This was accompanied by reduced cell numbers, viability, and apoptosis compared with LPS-treated controls (Fig. 2B–D; Supplemental Fig. S2E). *Max* knockout B cells also failed to proliferate when activated with IgM-μ or a combination of anti-CD40/ IL-4 ex vivo (Supplemental Fig. S2A–E). Similar effects on proliferation and cell size were observed in *Max*$^{fl/fl}$ lck-Cre CD3$^+$ T lymphocytes stimulated with anti-CD3 and anti-CD28 (Supplemental Fig. S2F,G).

To ascertain whether *Max* loss affects MYC-driven lymphomagenesis, we crossed our *Max* conditional allele with Eμ-*Myc* mice in which the *Myc* transgene is predominantly restricted to the B lymphoid lineage (Adams et al. 1985; Harris et al. 1988). While all of the Eμ-*Myc Max* WT animals developed B-cell lymphomas with a median survival of 97 d, none of the Eμ-*Myc Max* knockout mice developed lymphoma even out to 300 d (Fig. 2E, data not shown). Premalignant Eμ-*Myc* BM B-cell precursors exhibited developmental defects, including a block at the pre-B-cell stage (Langdon et al. 1986); however, our analysis of BM populations failed to show an expansion of a pre-B-cell population in Eμ-*Myc Max* knockout mice (Fig. 2F; Supplemental Table S1). In addition, B220$^+$ cells from Eμ-*Myc Max* knockout mice were smaller than Eμ-*Myc* controls and exhibited decreased total RNA content (Supplemental Fig. S2H,I). Augmented spleen size and splenocyte numbers are typical of Eμ-*Myc*-induced B-cell lymphomagenesis (Harris et al. 1988). Compared with Eμ-*Myc Max* knockout mice, Eμ-*Myc Max* WT mice exhibited increased spleen size and significantly increased numbers and cell size of total and B220$^+$ CD19$^+$ splenocytes (Fig. 2G–J). Eμ-*Myc Max* knockout B220$^+$ splenocytes also had an increased proportion of mature IgM- and IgD-positive B cells when compared with WT controls (Fig. 2K), indicating that the *Max* knockout cells do not exhibit the defects in differentiation characteristic of premalignant Eμ-*Myc* cells. These data demonstrate that Eμ-*Myc* lymphomagenesis is severely compromised in the absence of *Max*.

Max *loss affects E2F targets and proinflammatory pathways in B cells*

To determine the effects of *Max* loss on the transcriptional program of normal and Eμ-*Myc*-expressing B cells, we performed RNA sequencing (RNA-seq) using B220$^+$ cells of the four genotypes described above (normalized counts in Supplemental Table S2). Strikingly, *Max* deletion in normal B cells doesn't completely phenocopy *Myc* loss in B cells. First, MAX depletion does not perturb the expression of B-cell lineage transcription factors (Supplemental Fig. S3A), in contrast to MYC loss, which was shown previously to down-regulate expression of factors such as EBF and PAX5 (Vallespinós et al. 2011). Second, *Max* knockout B cells exhibit a significant up-regulation of genes involved in proinflammatory pathways (Fig. 3A; Supplemental Fig. S3B). *Max* knockout B220$^+$ cells were also consistently larger than controls (Supplemental Fig. S3C). Taken together, our data suggest that these cells are in a quasiactivated state, possibly related to the loss of repressive MAX dimers (e.g., MNT–MAX see below), compensating for the absence of MYC–MAX function. Interestingly, a majority of genes that exhibit decreased expression upon *Max* knockout are cell cycle-related (Fig. 3B) and include E2F targets. Consistent with the loss of GC cells (Fig.1H,I), a group of genes crucial for GC maintenance is also down-regulated in *Max* knockout B cells (Supplemental Fig. S3D). Not surprisingly, several gene sets that were significantly enriched for in our analysis overlapped with those reported recently in Max knockout B cells (Supplemental Fig. S3E,F; Pérez-Olivares et al. 2018). We think it is likely that any differences in the differentially expressed genes in our study compared with that of Pérez-Olivares et al. (2018) are due to the use of distinct Cre drivers (CD19 vs. mb1).

To identify direct MYC–MAX and MNT–MAX targets, we carried out genomic occupancy analysis using CUT&RUN (cleavage under targets and release using nuclease) on *Max* WT and knockout B cells. CUT&RUN sequencing uses a combination of antibody targeted

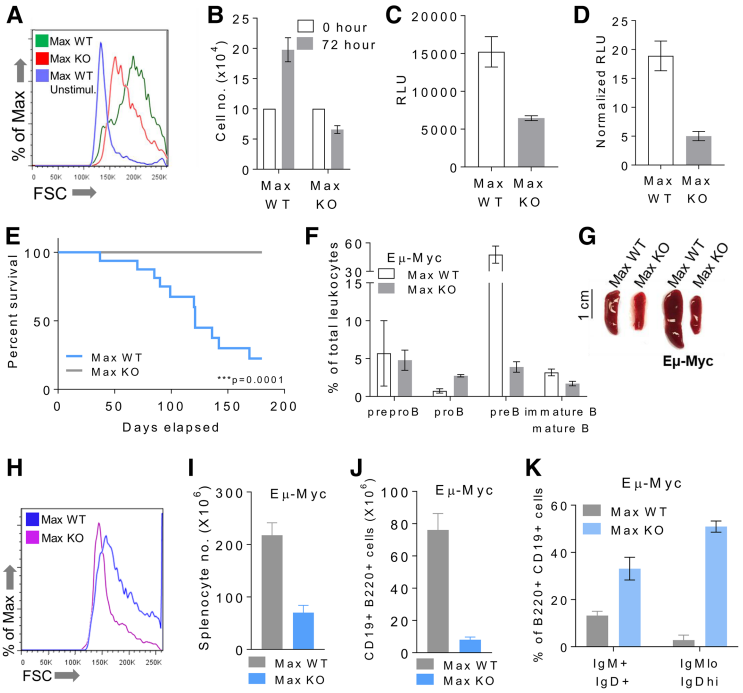

Figure 2. Requirement for *Max* in activated B cells and Eμ-*Myc*-induced lymphomagenesis. (*A*) Cell size as determined by forward scatter in WT unstimulated and LPS-activated *Max* WT and *Max* knockout (KO) B220$^+$ cells. (*B*) Cell number 72 h after treatment in LPS-treated *Max* WT and knockout ($n = 10$ from five WT and knockout mice). (*C*,*D*) Cell viability (*C*) and apoptosis (*D*) in LPS-activated B cells ($n = 9$ from three WT and knockout mice) assessed using luciferase-based Cell Titer Glo and Caspase Glo assays. (*E*) Kaplan-Meier curve showing survival analysis of Max WT ($n = 23$) and knockout ($n = 14$) Eμ-Myc animals up to 180 d. *P*-value was calculated using log-rank (Mantel-Cox) test. (*F*) Analysis of B-cell precursor populations in Eμ-*Myc* BM. (*G*) Representative spleens from normal and Eμ-*Myc* mice. (*H*) Histogram of cell size of Eμ-*Myc Max* WT and knockout mice. (*I*,*J*) Total splenocyte number (*I*) and CD19$^+$ B220$^+$ cell number (*J*) in Eμ-*Myc* WT and knockout mice. $n = 3$ for each. (*K*) Proportion on mature IgD-positive B cells in Eμ-*Myc* spleens. $n = 3$. All error bars represent SEM.

controlled cleavage and nuclease-based release of DNA fragments to analyze protein occupancy on DNA (Skene and Henikoff 2017; Janssens et al. 2018). Peaks that were called in two independent experiments were used for analysis. MAX was found to bind to ~11,000 gene loci (within ±5 kb of the transcription start site [TSS] or within the gene body) in WT B cells. There was an overall reduction in MAX and MNT binding in Max knockout cells when compared with WT (Fig. 3C). MYC occupancy appeared to be lower than MAX and MNT occupancy in WT B cells but was also markedly decreased in MAX-null B cells (Fig. 3C). The decrease in MAX binding at a representative gene (*Cbx5*) is shown in Figure 3D. The residual MAX binding observed in *Max* knockout B cells was most likely derived from a fraction of B cells that escaped Cre-mediated deletion of *Max* (~14%) (see Fig. 1E). In addition to the E-box motif, MEME and HOMER analysis revealed a significant enrichment for E2F motifs in MAX-bound regions in WT B cells compared with the IgG control (Fig. 3E; Supplemental Fig. S4A). We observed a substantial overlap between MAX, MYC, and MNT binding in WT B cells (Supplemental Fig. S4B; Supplemental Table S3). Gene set enrichment analysis revealed that cell cycle, E2F target, and MYC target gene sets were enriched for in the MNT–MAX–MYC-bound gene populations (Fig. 3F). Around 40% of inflammatory response-related genes appeared to be directly bound by MNT–MAX. Therefore, the effects of *Max* inactivation on up-regulation of inflammatory genes (Fig. 3A; Supplemental Fig. S3B) are likely direct.

When we correlated MAX occupancy with gene expression changes in *Max*-null cells, we found that ~76% of the genes down-regulated in *Max*-null cells were occupied by MAX in WT cells, while ~65% of up-regulated genes were directly bound by MAX (Fig. 3G). Remarkably, 84% of MAX-bound genes were not differentially expressed in *Max* knockout B cells, including the majority of MAX-bound E2F target genes. Expression of E2F1-3 and phosphorylation of Rb were also unaffected by *Max* loss (Supplemental Fig. S4C,D). The lack of change in expression of a majority of MAX-bound genes may be due to loss of binding by both the transcriptionally activating (MYC) and repressive (MXD, MNT, and MGA) heterodimerization partners of MAX and is consistent with the weak effects of MAX deletion on B-cell differentiation. Consistent with this idea, we observed that the expression of MYC and E2F target genes that are cobound by MYC, MNT, and MAX remained unchanged upon the deletion of *Max* (Supplemental Fig. S4E). Another possibility is that E2Fs themselves can compensate for loss of MYC–MAX at key promoters. Indeed, we see E2F1 occupancy at target genes *Cbx5* and *Ncl* in Max knockout cells, although at reduced levels. This is in contrast to the near elimination of MYC, MAX, and MNT occupancy (Fig. 3D; Supplemental Fig. S4F).

Max *loss destabilizes MYC protein*

To determine whether the gene expression changes and decreased MYC occupancy in *Max* knockout cells are solely due to the inability of MYC to bind DNA without MAX, we measured MYC levels in *Max* knockout B cells. While *Myc* mRNA levels were not affected by *Max* deletion (Fig. 4A), we observed a striking reduction in MYC protein levels in *MAX* knockout cells (Fig. 4B; Supplemental Fig. S4G). This result was surprising in light of previous studies indicating that MYC is subject to negative autoregulation in normal B cells (Grignani et al. 1990).

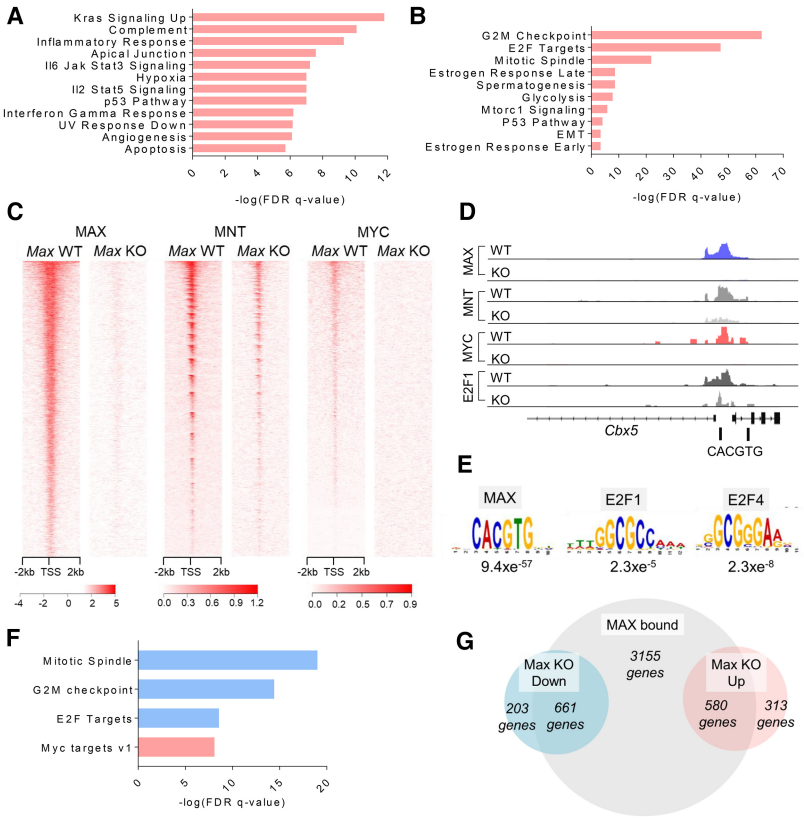

Figure 3. Gene expression profiling and genomic occupancy of MAX in B cells. (*A*,*B*) Hallmark gene set enrichment for pathways up-regulated (*A*) and down-regulated (*B*) in Max knockout (KO) B cells relative to WT B cells. (*C*) Next-generation sequencing (NGS) plots depicting genomic occupancy of MYC, MAX, MNT, and E2F1 in Max WT and knockout B cells ranked on expression changes. (*D*) Representative peaks for MAX, MYC, and MNT at E2F target *Cbx5*. (*E*) Motifs significantly enriched at MAX-bound genes. (*F*) Gene set enrichment for pathways enriched in MNT–MAX–MYC-bound genes. (*G*) Overlap of MAX-bound genes with genes that are differentially expressed in *Max* knockout B cells (false discovery rate <0.05 cutoff for differential expression).

Importantly, we found that treatment of B cells with the proteasomal inhibitor MG132 resulted in near-complete restoration of MYC levels in *Max* knockout B cells (Fig. 4C,D). Taken together, these results strongly suggest that MAX influences MYC stability.

Phosphorylation of AKT (p-AKT) and subsequent phosphorylation of GSK3β (p-GSK3β) at Ser9 is known to increase MYC stability (Cross et al. 1995; Farrell and Sears 2014). Because levels of both p-AKT Ser473 and p-GSK3β (Ser9) appeared to be higher in *MAX* knockout B cells (Supplemental Fig. S4D,H), we surmise that MAX loss regulates factors independent of GSK3β-mediated regulation of MYC stability. To obtain a snapshot of MYC stability at a single cell level, we stained splenic

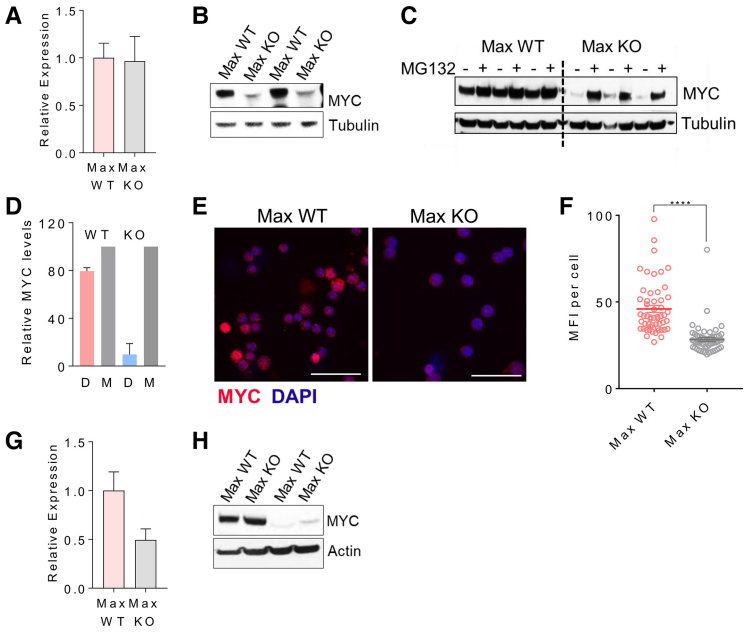

Figure 4. MYC stability upon MAX loss in normal and premalignant B cells. (*A*,*B*) mRNA (*A*) and protein (*B*) levels of *Myc* in WT and knockout (KO) B cells. $n = 4$ for WT and knockout. (*C*,*D*) Immunoblot (*C*) and quantification (*D*) of MYC levels following 2 h of MG132 treatment of *Max* WT and knockout B cells. $n = 3$ for WT and knockout. (*E*,*F*) Representative micrographs (*E*) and mean fluorescence intensity quantification (*F*) of MYC staining in sorted B220$^+$ splenocytes from Max WT and knockout mice. $n = 54$ WT cells; $n = 61$ knockout cells. Scale bar, 100 µm. (*G*,*H*) *Myc* mRNA levels (*G*) and MYC protein levels (*H*) in Eμ-*Myc* Max WT and knockout cells. All error bars represent SEM.

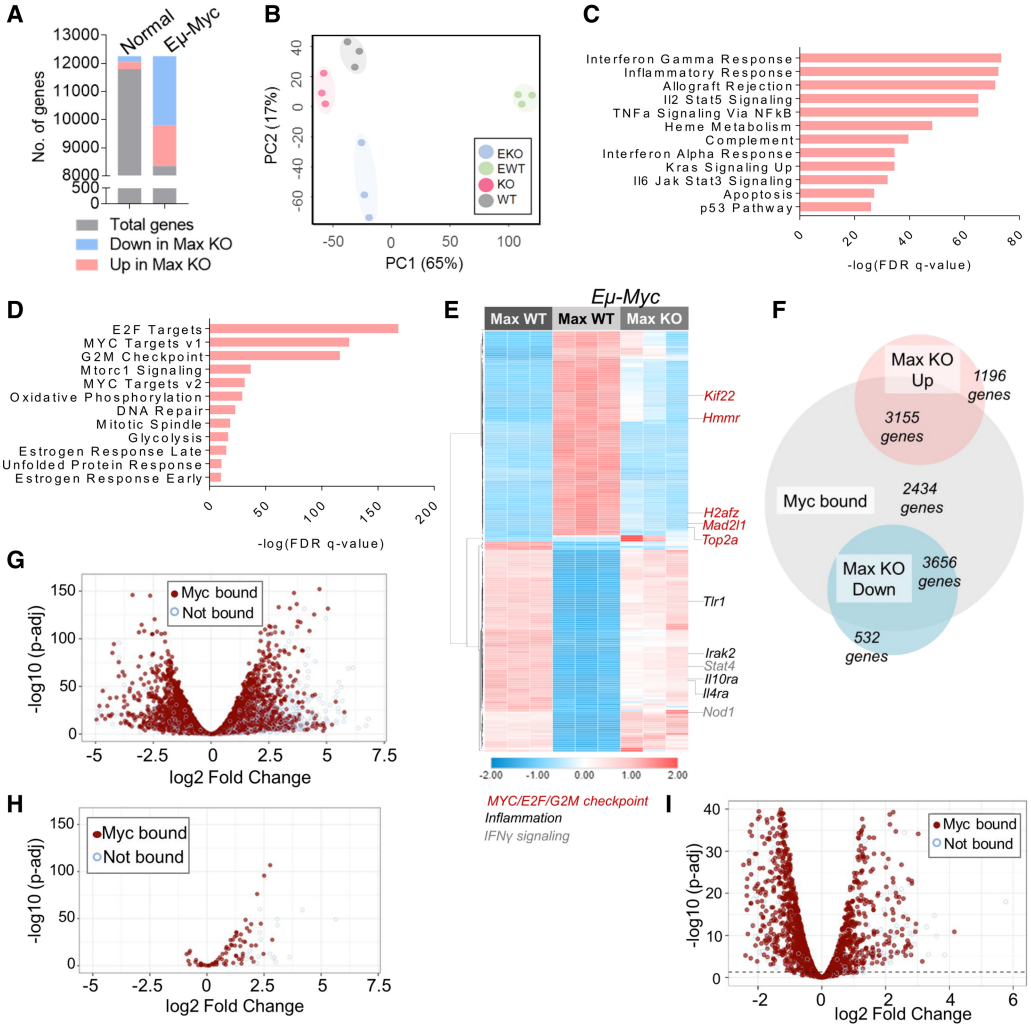

Figure 5. *Max* loss leads to a global down-regulation of the Myc signature in Eμ-*Myc* premaligant cells. (*A*) Summary of total differentially expressed genes in *Max* knockout normal and premalignant B cells. (*B*) Principal component analysis of all four genotypes. (EWT) Eu-*Myc Max* WT; (EKO) Eu-*Myc Max* knockout; (WT) *Max* WT; (KO) *Max* knockout. (*C*,*D*) Hallmark gene set enrichment for pathways up-regulated (*C*) and down-regulated (*D*) in Eu-*Myc* premalignant *Max* knockout B cells. (*E*) Heat map representation of global transcriptional changes in Eu-*Myc* premalignant *Max* WT and *Max* knockout cells. Representative genes from important categories are labeled. (*F*,*G*) Venn diagram (*F*) and volcano plot (*G*) of differentially expressed genes that are directly bound by MYC. (*H*,*I*) Volcano plots depicting the proportion of differentially expressed inflammation-related genes (*H*) and E2F target genes (*I*) that are directly bound by MYC in Eu-*Myc* premalignant cells.

B220$^+$ cells from Max WT and knockout mice to assess MYC protein levels and observed a significant reduction in MYC levels in cells from Max knockout mice, similar to immunoblots on whole-cell extracts (Fig. 4E,F; Supplemental Fig. S4I).

We next examined whether *Max* deletion in premalignant Eμ-*Myc* cells impacts MYC levels in a similar fashion. Although mRNA levels were reduced by 50% (Fig. 4G; Supplemental Fig. S5A), we observed a striking decrease in MYC protein levels and half-life (Fig. 4H; Supplemental Fig. S5B–D). Overall, this indicated that *Max* deficiency has a profound effect on MYC stability in both normal and premalignant settings.

Max *loss leads to a global down-regulation of the MYC signature in Eμ-*Myc*-expressing premalignant cells*

Given the profound effect on MYC protein levels, we hypothesized that the loss of MYC stability would have a widespread effect on the transcriptional profile of premalignant *Max*-null cells. Indeed, in contrast to normal B cells, where the loss of *Max* affects the expression of ~550 genes (twofold change cutoff, false discovery rate [FDR] <0.05), MAX depletion in Eμ-*Myc* mice causes a dramatic shift in the expression of thousands of genes (Fig. 5A), with Eμ-*Myc Max* WT cells occupying a space distinct from the other genotypes in a principle component analysis plot (Fig. 5B). Whereas genes up-regulated in

Eμ-*Myc Max* knockout cells showed a close alignment with signatures enriched in normal B cells lacking *Max* (Fig. 5C), genes down-regulated in Eμ-*Myc Max* knockout cells revealed a significant enrichment for MYC signatures (Fig. 5D). This translated to robust differences in expression where Eμ-*Myc Max* knockout and *Max* WT profiles closely resemble each other and are nearly the inverse of the Eμ-*Myc Max* WT (Fig. 5E). Interrogation of a publicly available ChIP-seq (chromatin immunoprecipitation [ChIP] combined with high-throughput sequencing) data set in B cells (Sabò et al. 2014) revealed that 73% of the genes known to be bound by MYC in Eμ-*Myc* premalignant cells are differentially expressed in Eμ-*Myc Max* knockout B220$^+$ cells (Fig. 5F,G; Supplemental Fig. S5E). We also observed that in contrast to normal B cells, a substantial proportion of MAX-regulated inflammation-related genes are directly bound by MYC (Fig. 5H). In addition, a large fraction of MYC-bound E2F targets (Fig. 5I; Kuleshov et al. 2016) are down-regulated in Eu-*Myc Max* knockout cells. This may be due partly to the decrease in E2F1-3 expression in knockout cells (Supplemental Fig. S5F).

MAX loss or inhibition of MYC–MAX dimerization results in repression of MYC stability factors

Since MAX loss appeared to have a significant impact on MYC stability, we wanted to identify effectors downstream from MYC–MAX that may form a positive feedback loop to maintain MYC protein levels. While MYC proteins generally have short half-lives (on the order of 20–30 min), MYC half-life increases in several Burkitt's lymphoma lines and ES cells (Hann and Eisenman 1984; Gregory and Hann 2000; Cartwright et al. 2005). The rate of MYC protein degradation is mediated by several factors that interfere with signals triggering MYC ubiquitination and proteasomal degradation (Farrell and Sears 2014). We noted in our RNA-seq data that genes encoding MYC stability factors, including *Btrc*, *Cip2a*, and *Set*, are up-regulated in Eμ-*Myc* cells relative to normal B220$^+$ cells and down-regulated in Eμ-*Myc Max* knockout B cells (Fig. 6A). Moreover, the promoters of these genes are directly bound by MYC in premalignant cells (Fig. 6B; Supplemental Fig. S6A). CIP2A and SET are inhibitors of protein phosphatase 2A (PP2A), which normally dephosphorylates the stabilizing phospho-Ser62 (S62) within the conserved Myc box 1 phospho-degron. CIP2A and SET are often overexpressed in tumors and block PP2A activity, resulting in persistence of phospho-S62 and MYC (Junttila et al. 2007; Junttila and Westermarck 2008; Wiegering et al. 2013). BTRC functions to enhance MYC stability via ubiquitylation (Popov et al. 2010).

To confirm whether these genes are regulated by MYC–MAX in tumor lines, we treated Daudi and P493 human B-cell lymphoma lines (Schuhmacher et al. 2001) with 10058-F4 (referred to here as Myci), a small molecule reported to inhibit MYC–MAX heterodimerization (Yin et al. 2003). We observed a decrease in MYC protein levels, accompanied by reduced proliferation and a down-regulation of the stability factors in Myci-treated cells (Fig. 6C; Supplemental Fig. S6B–E). While *Myc* RNA levels were only moderately reduced (Supplemental Fig. S6F), MYC phospho-Ser62 levels were nearly eliminated upon Myci treatment (Fig. 6D). In addition, a time course of MYC degradation following cycloheximide treatment in P493-6 cells revealed that MYC half-life is reduced in Myci-treated cells (Supplemental Fig. S6G,H).

Similar results were obtained in HCT116 colon adenocarcinoma cells, where proliferation and MYC protein levels were diminished upon treatment with Myci (Fig. 6E–G). To extend this analysis, we used PSN1 pancreatic and NCI-H23 lung adenocarcinoma human tumor lines and observed similar effects (Supplemental Fig. S7A–D). Consistent with genomic occupancy data in Eμ-*Myc* cells, ENCODE data show that MAX is directly associated with the promoter-proximal regions of the *BTRC*, *CIP2A*, and *SET* genomic loci in HCT116 cells (Supplemental Fig. S7E). To rule out the possibility that the MYC stability phenotype is specific to 10058-F4, we used the MS-008 probe that promotes homodimerization of MAX and also observed decreased MYC protein levels. This is consistent with a recent study showing the same effect on MYC stability (Supplemental Fig. S7F–H; Struntz et al. 2019). In addition, induction of Omomyc, a peptide that binds to MYC's bHLH region, also led to decreased MYC protein levels, suggesting that the effect on MYC stability is not due to a lack of binding at its dimerization interface (Fig. 6H,I; Supplemental Fig. S7I; Beaulieu et al. 2019).

MYC degradation in inhibitor-treated cells is dependent on FBW7 and phosphorylation of MYC T58

To confirm that the decrease in MYC protein levels is indeed through the loss of multiple stability factors that affect *Fbw7* activity, we examined MYC levels in HCT116 colon cancer cells lacking the *FBW7* ubiquitin ligase known to target MYC for degradation (Welcker et al. 2004; Yada et al. 2004). We found that MYC turnover in FBW7$^{-/-}$ HCT116 is largely unaffected by treatment with the dimerization inhibitor compared with the rapid turnover in control HCT116 cells treated with inhibitor (Fig. 7A–C). Moreover, CIP2A levels are unchanged in FBW7-null cells upon Myci treatment, whereas they decrease in Myci-treated WT HCT116 cells (Fig. 7D; Supplemental Fig. S7J). This supports the notion that disruption of MYC–MAX dimerization does not affect MYC–MAX-mediated transcription alone; it also augments degradation of MYC in cells. Our data suggest that the activity of the FBW7–SCF ubiquitin complex significantly contributes to the decreased stability of MYC.

To complement these data, we asked whether overexpression of a T58A phospho-site mutant would have a similar effect. We ectopically expressed either MYC or MYC^{T58A} in HCT116 cells and treated them with a higher concentration (75 μM) of Myci to compensate for higher levels of MYC in these cells. Cells were harvested after 24 h, and we found that MYC^{T58A}-expressing cells maintained higher levels of MYC and CIP2A expression upon Myci treatment when compared with MYC-expressing controls (Fig. 7E,F; Supplemental Fig. S7K).

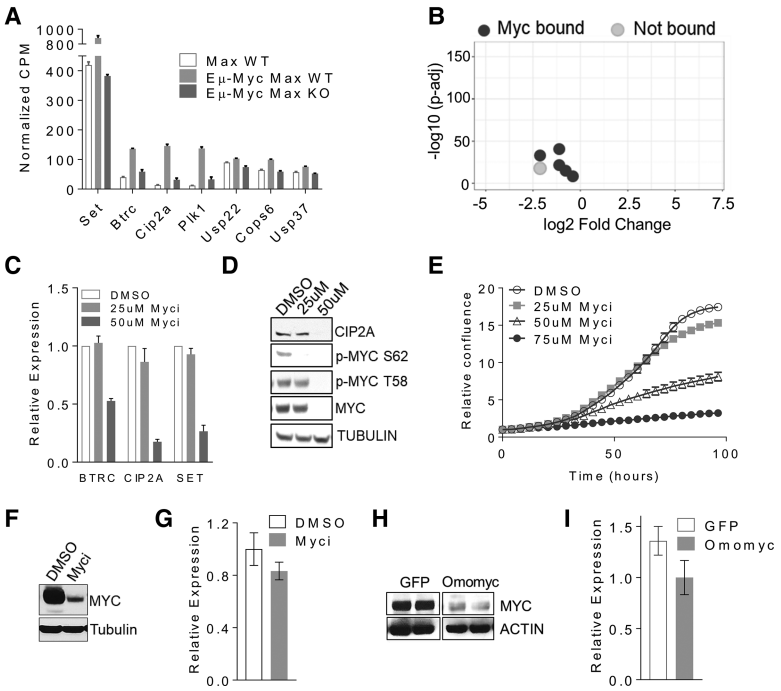

Figure 6. Factors mediating MYC degradation in the absence of MAX. (*A*) Normalized expression values of MYC-stabilizing genes in WT and Eμ-*Myc* B220$^+$ cells. (*B*) Volcano plot showing expression changes for MYC stability genes and ChIP binding data for MYC in premalignant Eμ-*Myc* B220$^+$. (*C*) qPCR for *BTRC*, *CIP2A*, and *SET* in DMSO- and Myci (10058-F4)-treated Daudi cells. (*D*) Western blot for pMYC S62 and CIP2A levels in Myci-treated Daudi cells. (*E*) Growth curves for HCT116 cells at different concentrations of Myci. (*F*) Western blot showing MYC levels in Myci-treated HCT116 cells. (*G*) MYC RNA levels in Myci-treated HCT116 cells. (*H*,*I*) Representative immunoblot of MYC levels (*H*) and MYC mRNA levels (*I*) in Omomyc- versus GFP-expressing HCT116 cells. All error bars represent SEM.

Last, we asked whether the MYC paralogs N-MYC and L-MYC are also destabilized by loss of heterodimerization. A previous study reported a decrease in N-MYC in SKNBE neuroblastoma cells treated with 10058-F4 (Zirath et al. 2013). We extended our analysis to another *Mycn*-amplified neuroblastoma line (IMR-32) and the *Mycl*-amplified small cell lung cancer line NCI-H2141. Treatment with Myci leads to a reduced growth and a decrease in N-MYC and L-MYC protein, respectively (Supplemental Fig. S8A–D).

Discussion

Our in vivo studies on *Max* loss in normal B cells and Eμ-*Myc*-driven lymphomagenesis offer several insights into the context-dependent function of MAX. Surprisingly, the major hallmarks of normal B-cell differentiation are largely unperturbed by *Max* loss. The fact that MYC protein is destabilized and nearly absent in the *Max*-null B cells makes it unlikely that MYC is functioning independently of MAX. The likely scenario is that in *Max* knockout cells, loss of repressive MAX–MXD heterodimers may serve to partially compensate for diminished MYC activity. For example, MNT binds thousands of promoters in normal B cells, and its binding is partially attenuated in MAX knockout cells (Fig. 3C). This alleviation of repression may also underlie the indirect activation of proinflammatory pathways in *Max*-null B cells, although it is certainly possible that loss of MYC–MAX activation might also contribute to this phenotype (Casey et al. 2016). Several lines of evidence suggest that the loss of repressive heterodimers might partly rescue the loss of MYC–MAX. First, deletion of *Myc* in B cells has a similar yet more severe phenotype than the one that we observed upon depletion of *Max* (Habib et al. 2007; Vallespinós et al. 2011; Pérez-Olivares et al. 2018). Second, this result is similar to that seen upon inactivation of MAX in *Drosophila melanogaster*, where larval development is less compromised by loss of MAX than by loss of MYC (Steiger et al. 2008). Moreover, the arrest of larval growth as a result of MYC deletion is partially rescued by loss of MNT. Another possibility is that the requirement for MYC activity is rather minimal or readily compensated for by factors such as E2Fs in normal B-cell progenitors. This is reasonable because a significant overlap between E2F- and MYC-regulated genes has been noted in several systems. For example, MYC drives proliferation in *E2f1-3*-deficient retinal progenitor cells (Chen et al. 2009). Similarly, combined deletion of *Myc* and *E2f1-3* disrupts crypt villus integrity in the intestine, whereas neither *Myc* ablation nor *E2f1-3* ablation alone has an effect (Liu et al. 2015). Our own data suggest a similar compensatory mechanism might exist in B cells, as E2F1 still binds E2F targets such as *Cbx5* and *Ncl* even upon *Max* deletion.

However, we did observe nominal effects on normal B-cell development upon B-cell-specific deletion of *Max*. This is evidenced by decreased B-cell population sizes in both the BM and spleen, with a nearly complete loss of GC cells in the latter. Overall, our findings suggest that MYC–MAX genomic binding and transcriptional activity is not absolutely required for several key aspects of early B-cell differentiation. Nonetheless, deletion of *Max* attenuates certain processes where MYC is critically required, such as GC formation.

Consistent with the GC phenotype, we observed a heightened requirement for *Max* in situations where MYC levels are elevated. *Max*-null B cells fail to grow in size or proliferate upon ex vivo stimulation with agents such as LPS and CD40/Il-4. In the context of Eμ-*Myc*,

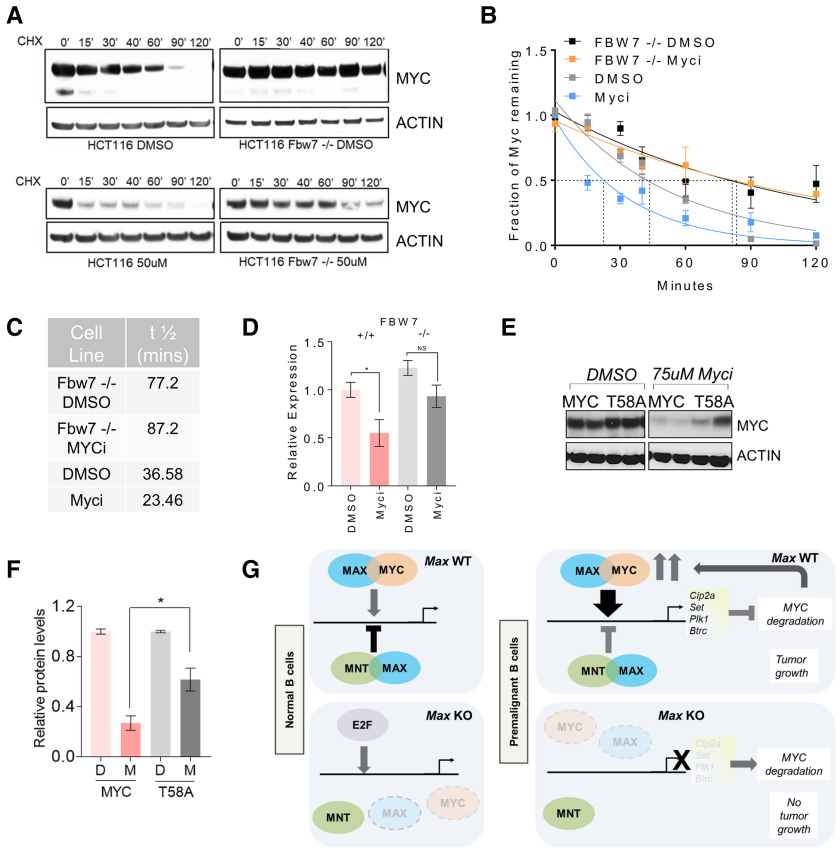

Figure 7. MYC degradation in FBW7$^{-/-}$ and MYC phospho-mutant-expressing cells. (*A*) Representative blot for MYC levels in HCT116 and HCT116 FBW7$^{-/-}$ cells following a cycloheximide chase. (*B*) Determination of MYC half-life in Myci-treated control and FBW7$^{-/-}$ cells. $n=3$ experiments. (*C*) Half-life of MYC under each of the four conditions. (*D*) qPCR for CIP2A levels in HCT116 cells. $n=3$. $P=0.048$ for Myci versus control in WT. (*E*) Immunoblot of MYC levels following treatment with 75 µM Myci in MYC- or MYC^{T58A}-overexpressing HCT116 cells. (*F*) Quantification of MYC levels following MYCI treatment in MYC- versus MYC^{T58A}-expressing HCT116. $n=3$ for each condition. All error bars represent SEM. (*G*) Model depicting proposed network dynamics in normal B cells and premalignant Eµ Myc cells and the consequences of *Max* deletion in each context. In normal B cells, MNT–MAX activity largely balances MYC–MAX activity, leading to the activation of only a subset of MYC target genes. Upon *Max* loss, alleviation of MNT–MAX repression and E2F activation of target genes partially compensates for loss of MYC–MAX activity. In premalignant cells, MYC–MAX heterodimers show increased activity and activate MYC-stabilizing genes such as Cip2a and Set. Disruption of this circuit via *Max* deletion leads to destabilization of MYC protein and loss of the MYC signature expression. Hence, no tumors arise in knockout mice.

depletion of *Max* leads to an unstable pool of MYC and largely reverses the transcriptional effects of MYC, leading to complete abrogation Eµ-*Myc*-driven lymphomagenesis. In addition, we found evidence for MYC–MAX cooperation with E2F factors in driving the proliferation of premalignant B cells. *Max* loss leads to a down-regulation of *E2f1-3* and subsequent expression changes of several E2F targets. The inability of Eµ-*Myc Max* knockout B220^{+} cells to undergo malignant transformation strongly suggests that *Myc*-driven tumorigenesis in vivo absolutely requires *Max*. This is in contrast to cancers such as GIST (gastrointestinal stromal tumors), where *Max* loss drives proliferation (Schaefer et al. 2017). A similar tumor-suppressive role has been ascribed to *Max* in SCLC (Romero et al. 2014). Based on our results, it is reasonable to assume that these tumors are not dependent on MYC for their growth. Indeed, inactivating mutations of *MAX* are mutually exclusive with *MYC* paralog amplifications (Romero et al. 2014). In such a situation, MXD–MAX genomic binding and repression might be more widespread than MYC–MAX activity. Hence, *MAX* loss in these tumors could conceivably lead to derepression at subsets of E-box-containing promoters, resulting in activation of pro-oncogenic pathways.

Our experiments across a broad spectrum of tumor lines revealed that disruption of MYC–MAX dimerization has an effect on MYC stability similar to those seen in vivo. This is accompanied by a decrease in expression of genes that promote MYC stability. In addition, we observed that MYC degradation is reduced in inhibitor-treated FBW7$^{-/-}$ or MYC T58A cells. Taken together, these data indicate that MYC stability is at least partially regulated via an FBW7-dependent degradation pathway. Recent studies have shown that MYC forms phase-separated structures on chromatin (Boija et al. 2018). Failure to dimerize with MAX might hinder MYC's ability to form such higher-order complexes or phase-separated structures. This in turn could expose lysines in MYC that may contribute to enhanced MYC degradation. Regardless of the mechanism, these findings suggest that specific MYC–MAX dimerization inhibitors will be doubly efficacious, targeting both MYC-driven transcription and MYC protein levels. By eliminating MYC, dimerization inhibitors would suppress transcription-independent functions of MYC, such as those mediated by MYC-nick (Conacci-Sorrell et al. 2010). This additional layer of autoregulation of MYC stability is likely to have broad mechanistic consequences during tumor initiation. Our data lend support to the notion that transcriptional up-regulation of PP2A inhibitors by MYC may lead to enhanced MYC stability and function in premalignant settings to facilitate transformation even in the absence of genomic alterations of *Myc* (Junttila and Westermarck 2008; Khanna et al. 2009). It will therefore be important to closely examine

the consequences of MYC inhibition in cancers where PP2A is lost and/or regulators such as CIP2A and SET are overexpressed. However, it is also possible that MYC activation of several factors simultaneously reinforces MYC stability so deregulation of any one factor might not be sufficient to reduce MYC levels.

In summary, our data suggest that loss of *Max* in vivo disables MYC activity through inhibition of direct MYC association with genomic DNA and through destabilization of the MYC protein itself. We surmise that increased MYC degradation is facilitated at least in part by decreased MYC–MAX activity at the promoters of genes such as *Cip2a*, whose protein products normally serve to stabilize MYC by attenuating FBW7-mediated proteasomal degradation (Fig. 7G; Junttila et al. 2007). In this scenario, MYC–MAX heterodimers drive a feed-forward circuit that reinforces high MYC expression in tumors as diverse as B-cell lymphomas and colon adenocarcinomas. In fact, a recent study shows that MYC regulates the kinase *Plk1* to maintain its stability in an aggressive form of lymphoma (Ren et al. 2018). In colorectal cancer, MYC has been shown to activate USP28, a deubiquitinase that in turn stabilizes MYC, JUN, and NOTCH (Diefenbacher et al. 2014). Disruption of this circuit (for example, in Eμ-*Myc Max*-null B cells) results in loss of MYC protein expression and a complete abrogation of lymphomagenesis. In the case of normal B cells, where MYC activity might partially be compensated for loss of MXD–MAX interactions, this feedback regulation might not be as crucial except in contexts where B cells are activated (Fig. 7G). Taken together, our data underscore the complex circuitry and the integrated context-dependent functions of MAX and the broader MYC network.

Materials and methods

Mouse strains and tissue processing

All mice were housed and treated according to the guidelines provided by the Fred Hutchinson Institutional Animal Care and Use Committee. For *Max* conditional mice, clonal G418R targeted ES cell lines were produced, and integration of the targeting vector was verified by genomic PCR and Southern blotting. Eμ-*Myc* mice were purchased from Jackson Laboratories. $Max^{fl/fl}$, mb1-cre, lck-cre, and Eμ-*Myc* mice were maintained on a mixed 129/C57BL6 background after crossing. For BM studies, cells from 5- to 10-wk-old mice were flushed from femurs and tibiae using a 27.5-gauge needle under sterile conditions for subsequent use in stimulation experiments and flow cytometric analyses. Spleens and thymic tissue were harvested under aseptic conditions from 5- to 10-wk-old mice, and single-cell suspensions were made for isolation of purified populations. For immunohistochemistry and immunofluorescence, spleens were fixed in formalin and embedded in paraffin blocks.

Cell culture and in vitro experiments

Daudi, P493-6, and SKNBE cells were grown in RPMI with 10% FBS. NCI-H23, PSN-1, HCT116, PT67, and 293FT lines were maintained in DMEM with 10% FBS. NCI-H2141 cells were cultured in DMEM with 20% FBS supplemented with insulin and pyruvate. For MYC and MYC T58A expression, retrovirus was made using the PT67 packaging line with pBabe-puro-MYC and pBabe-puro-MYCT58A retroviral constructs. HCT116 cells were then transduced with pBabe-puro-MYC and pBabe-puro-MYCT58A retrovirus, and experiments were performed after puromycin selection for at least 3 d. For Omomyc studies, pSLIK-hygro-OMOMYC and pSLIK-hygroGFP lentiviral particles were made using 293FT cells and p-VSV-G and pPAX2 packaging vectors. HCT116 cells were transduced, and experiments were performed after 100-μg/mL hygromycin selection for 1 wk. Omomyc expression was induced by treatment with 2 μg/mL doxycycline for 2 d.

Flow cytometry and cell sorting

For B-cell developmental studies, cells harvested from the BM and spleen were stained with fluorochrome-conjugated antibodies against B-cell lineage-specific markers (B220, CD19, IgM, and CD43), pan-T-cell marker CD3, and myeloid marker CD11b. Viability was assessed using DAPI, and leukocytes were gated upon using forward and side scatter parameters. For mature B-cell population studies, splenocytes were stained with fluorochrome-conjugated antibodies against B220, CD19, IgM, and IgD. B cells were sorted from spleens using AutoMACS mouse $B220^+$ beads. Purified $B220^+$ cells were then used for imaging, ex vivo stimulation, RNA-seq, and CUT&RUN experiments. For T lymphocyte studies, thymocytes were stained with antibodies against CD4 and CD8. All populations were analyzed on a BD FACS Canto II. See Supplemental Table S4 for details on the antibodies used.

Cell growth assays

Trypan blue-negative cells were counted at fixed time points to assess cell growth. Cell Titer Glo and Caspase Glo luciferase assays (Promega) were used to assess cell growth and apoptosis for ex vivo stimulated B cells. For growth curves of adherent cell lines, cells were seeded in 96-well dishes and imaged at fixed time intervals on either an Incucyte S3 or Incucyte zoom. Percent confluence was used as a measure of cell growth.

Immunohistochemistry and immunofluorescence

Immunohistochemistry was performed on 5-μm-thick paraffin-embedded mouse spleen sections. Following heat-induced antigen retrieval, sections were incubated with primary antibodies followed by Alexa-conjugated secondary antibodies (Invitrogen). For immunofluorescent staining, sorted cells were cytospun on charged slides and fixed in 4% formaldehyde. Following primary incubation, Alexa-conjugated secondary antibodies (Invitrogen) were used, and slides were mounted using Prolong Gold antifade with DAPI. Images were acquired using a Nikon E800 microscope, and image analysis and intensity measurements were performed using ImageJ. See Supplemental Table S4 for a list of the antibodies used.

Western blots and inhibitor studies

For Western blots, cells were lysed in RIPA buffer with protease and phosphatase inhibitors and reduced in LDS buffer. For inhibitor studies, cells were treated with the MYC inhibitor 10058-F4 or the Max probe MS-008 for 2 d prior to harvest unless noted otherwise. For cycloheximide chase experiments, cells were treated with 5 μg/μL cycloheximide and immediately lysed in RIPA buffer at specified time points. For MG132 studies, cells were treated with 10 μM MG132 for 2 h prior to lysis. Densitometry for all

blots was performed using ImageJ. See Supplemental Table S4 for details on the antibodies used.

qRT-PCR, RNA-seq, and analysis

All RNA isolation was performed using the Direct-zol RNA miniprep kit (Zymoresearch). For qRT-PCR, 500 ng to 2 µg of input total RNA was used, cDNA was generated using the Revertaid cDNA synthesis kit (Thermo Fisher), and a Bio-Rad iCycler was used. Either SYBR Green or FAM probe-based methods were used. For RNA-seq, $B220^+$ cells were purified using $B220^+$ microbeads (AutoMACS) from spleens of 5- to 6-wk-old mice from all genotypes. Following RNA isolation, total RNA integrity was checked using an Agilent 4200 TapeStation and quantified using a Trinean DropSense96 spectrophotometer (Caliper Life Sciences). Libraries were prepared using the TruSeq version 2 RNA sample preparation kit with 500 ng of input RNA. Paired-end sequencing was performed on an Illumina HiSeq 2500. Reads that didn't pass Illumina's base call quality threshold were removed. Reads were then aligned to mm10 mouse reference genome using TopHat version 2.1.0. Counts were generated for each gene using htseq-count version 0.6.1p1 (using the "intersection-strict" overlapping mode). Genes that didn't have at least one count per million in at least three samples were removed. Data were normalized, and comparisons were conducted using the exact test method in edgeR version 3.18.1. Gene ontology analysis was performed using hallmark data sets on mSigDB (Subramanian et al. 2005; Liberzon et al. 2015). Heat maps were generated using Morpheus (https://software.broadinstitute.org/morpheus).

CUT&RUN studies

For chromatin occupancy studies, primary mouse B cells isolated from spleens were prepared fresh. Cells were bound to ConA beads, permeabilized, and incubated overnight with antibodies against MYC, MAX, MNT, and E2F1. One million cells were used per immunoprecipitation, and the CUT&RUN protocol was followed (Janssens et al. 2018). Using an Illumina HiSeq 2500 instrument, 25 × 25 paired-end sequencing was performed (5 million–10 million reads), and sequences were aligned to the mm10 reference genome assembly using Bowtie2.

Normalization was performed based on library size. Peak calling used a threshold peak calling script to differentiate signal to noise (Kasinathan et al. 2014). This processing was carried out with Bedtools, custom R scripts defining genome position, and the GenomicRanges R package. Peaks were identified as being associated with a gene if they were within ±5 kb from the TSS. For MYC, MNT, and MAX peak calling in WT B cells, peaks called in two independent experiments were intersected to mitigate background issues. Genomic plots were made using ngs.plot (Shen et al. 2014) or the R package ggplot2. Heat maps for genomic binding were made ranking genes according to log fold change in expression from the RNA-seq experiment. De novo enrichment for sequence specificity was determined using Homer (Heinz et al. 2010) and MEME-ChIP (Machanick and Bailey 2011).

Data availability

MYC-binding data from premalignant cells were obtained from Sabò et al. (2014) (Gene Expression Omnibus [GEO] accession no. GSE51004; https://www.ncbi.nlm.nih.gov/geo/query/acc.cgi?acc=GSE51004). RNA-seq data from this study are available from GEO under accession number GSE132773. CUT&RUN data from this study are available from GEO under accession number GSE132967.

Acknowledgments

We thank Nayanga Thirimanne, Bruce Clurman, Arnaud Augert, David MacPherson, Shelli Morris, Sergio Nasi, Nan Hyung Hong, and Patrick Carroll for providing essential reagents. We are grateful to Arnaud Augert, David MacPherson, and Brian Iritani for their critical reading of the manuscript. We also acknowledge the Genomics, Scientific Imaging, Flow Cytometry, and Experimental Histopathology scientific resources at Fred Hutchinson Cancer Research Center. This work was supported by National Institutes of Health/National Cancer Institute grants RO1 CA057138 and R35 CA 231989 (to R.N.E.).

Author contributions: H.M. and R.N.E. designed the study and cowrote the manuscript. H.M., P.-F.C., E.B., and J.T.C. performed and analyzed experiments. B.F. provided bioinformatics support and analyzed CUT&RUN data. D.J. and S.H. provided essential reagents and executed the CUT&RUN experiments. All authors discussed the results and read the manuscript.

References

Adams JM, Harris AW, Pinkert CA, Corcoran LM, Alexander WS, Cory S, Palmiter RD, Brinster RL. 1985. The c-myc oncogene driven by immunoglobulin enhancers induces lymphoid malignancy in transgenic mice. *Nature* **318:** 533–538. doi:10.1038/318533a0

Amati B, Brooks MW, Levy N, Littlewood TD, Evan GI, Land H. 1993. Oncogenic activity of the c-Myc protein requires dimerization with Max. *Cell* **72:** 233–245. doi:10.1016/0092-8674(93)90663-B

Beaulieu ME, Jauset T, Massó-Vallés D, Martínez-Martín S, Rahl P, Maltais L, Zacarias-Fluck MF, Casacuberta-Serra S, Serrano Del Pozo E, Fiore C, et al. 2019. Intrinsic cell-penetrating activity propels Omomyc from proof of concept to viable anti-MYC therapy. *Sci Transl Med* **11:** eaar5012. doi:10.1126/scitranslmed.aar5012

Blackwood EM, Eisenman RN. 1991. Max: a helix–loop–helix zipper protein that forms a sequence-specific DNA-binding complex with Myc. *Science* **251:** 1211–1217. doi:10.1126/science.2006410

Blackwood EM, Luscher B, Eisenman RN. 1992. Myc and Max associate in vivo. *Genes Dev* **6:** 71–80. doi:10.1101/gad.6.1.71

Boija A, Klein IA, Sabari BR, Dall'Agnese A, Coffey EL, Zamudio AV, Li CH, Shrinivas K, Manteiga JC, Hannett NM, et al. 2018. Transcription factors activate genes through the phase-separation capacity of their activation domains. *Cell* **175:** 1842–1855.16. doi:10.1016/j.cell.2018.10.042

Calado DP, Sasaki Y, Godinho SA, Pellerin A, Kochert K, Sleckman BP, de Alboran IM, Janz M, Rodig S, Rajewsky K. 2012. The cell-cycle regulator c-Myc is essential for the formation and maintenance of germinal centers. *Nat Immunol* **13:** 1092–1100. doi:10.1038/ni.2418

Carroll PA, Freie BW, Mathsyaraja H, Eisenman RN. 2018. The MYC transcription factor network: balancing metabolism, proliferation and oncogenesis. *Front Med* **12:** 412–425. doi:10.1007/s11684-018-0650-z

Cartwright P, McLean C, Sheppard A, Rivett D, Jones K, Dalton S. 2005. LIF/STAT3 controls ES cell self-renewal and pluripotency by a Myc-dependent mechanism. *Development* **132:** 885–896. doi:10.1242/dev.01670

Casey SC, Tong L, Li Y, Do R, Walz S, Fitzgerald KN, Gouw AM, Baylot V, Gutgemann I, Eilers M, et al. 2016. MYC regulates the antitumor immune response through CD47 and PD-L1. *Science* **352:** 227–231. doi:10.1126/science.aac9935

Chen D, Pacal M, Wenzel P, Knoepfler PS, Leone G, Bremner R. 2009. Division and apoptosis of E2f-deficient retinal progenitors. *Nature* **462:** 925–929. doi:10.1038/nature08544

Comino-Méndez I, Gracia-Aznárez FJ, Schiavi F, Landa I, Leandro-García LJ, Letón R, Honrado E, Ramos-Medina R, Caronia D, Pita G, et al. 2011. Exome sequencing identifies MAX mutations as a cause of hereditary pheochromocytoma. *Nat Genet* **43:** 663–667. doi:10.1038/ng.861

Conacci-Sorrell M, Ngouenet C, Eisenman RN. 2010. Myc-nick: a cytoplasmic cleavage product of Myc that promotes α-tubulin acetylation and cell differentiation. *Cell* **142:** 480–493. doi:10.1016/j.cell.2010.06.037

Conacci-Sorrell M, McFerrin L, Eisenman RN. 2014. An overview of MYC and its interactome. *Cold Spring Harb Perspect Med* **4:** a014357. doi:10.1101/cshperspect.a014357

Cross DA, Alessi DR, Cohen P, Andjelkovich M, Hemmings BA. 1995. Inhibition of glycogen synthase kinase-3 by insulin mediated by protein kinase B. *Nature* **378:** 785–789. doi:10.1038/378785a0

Diefenbacher ME, Popov N, Blake SM, Schülein-Völk C, Nye E, Spencer-Dene B, Jaenicke LA, Eilers M, Behrens A. 2014. The deubiquitinase USP28 controls intestinal homeostasis and promotes colorectal cancer. *J Clin Invest* **124:** 3407–3418. doi:10.1172/JCI73733

Farrell AS, Sears RC. 2014. MYC degradation. *Cold Spring Harb Perspect Med* **4:** a014365. doi:10.1101/cshperspect.a014365

Gregory MA, Hann SR. 2000. c-Myc proteolysis by the ubiquitin-proteasome pathway: stabilization of c-Myc in Burkitt's lymphoma cells. *Mol Cell Biol* **20:** 2423–2435. doi:10.1128/MCB.20.7.2423-2435.2000

Grignani F, Lombardi L, Inghirami G, Sternas L, Cechova K, Dalla-Favera R. 1990. Negative autoregulation of c-myc gene expression is inactivated in transformed cells. *EMBO J* **9:** 3913–3922. doi:10.1002/j.1460-2075.1990.tb07612.x

Habib T, Park H, Tsang M, de Alboran IM, Nicks A, Wilson L, Knoepfler PS, Andrews S, Rawlings DJ, Eisenman RN, et al. 2007. Myc stimulates B lymphocyte differentiation and amplifies calcium signaling. *J Cell Biol* **179:** 717–731. doi:10.1083/jcb.200704173

Hann SR, Eisenman RN. 1984. Proteins encoded by the human c-myc oncogene: differential expression in neoplastic cells. *Mol Cell Biol* **4:** 2486–2497. doi:10.1128/MCB.4.11.2486

Harris AW, Pinkert CA, Crawford M, Langdon WY, Brinster RL, Adams JM. 1988. The E mu-myc transgenic mouse. A model for high-incidence spontaneous lymphoma and leukemia of early B cells. *J Exp Med* **167:** 353–371. doi:10.1084/jem.167.2.353

Heinz S, Benner C, Spann N, Bertolino E, Lin YC, Laslo P, Cheng JX, Murre C, Singh H, Glass CK. 2010. Simple combinations of lineage-determining transcription factors prime *cis*-regulatory elements required for macrophage and B cell identities. *Mol Cell* **38:** 576–589. doi:10.1016/j.molcel.2010.05.004

Hobeika E, Thiemann S, Storch B, Jumaa H, Nielsen PJ, Pelanda R, Reth M. 2006. Testing gene function early in the B cell lineage in mb1-cre mice. *Proc Natl Acad Sci* **103:** 13789–13794. doi:10.1073/pnas.0605944103

Hopewell R, Ziff EB. 1995. The nerve growth factor-responsive PC12 cell line does not express the Myc dimerization partner Max. *Mol Cell Biol* **15:** 3470–3478.

Janssens DH, Wu SJ, Sarthy JF, Meers MP, Myers CH, Olson JM, Ahmad K, Henikoff S. 2018. Automated in situ chromatin profiling efficiently resolves cell types and gene regulatory programs. *Epigenetics Chromatin* **11:** 74. doi:10.1186/s13072-018-0243-8

Junttila MR, Westermarck J. 2008. Mechanisms of MYC stabilization in human malignancies. *Cell Cycle* **7:** 592–596. doi:10.4161/cc.7.5.5492

Junttila MR, Puustinen P, Niemelä M, Ahola R, Arnold H, Böttzauw T, Ala-aho R, Nielsen C, Ivaska J, Taya Y, et al. 2007. CIP2A inhibits PP2A in human malignancies. *Cell* **130:** 51–62. doi:10.1016/j.cell.2007.04.044

Kasinathan S, Orsi GA, Zentner GE, Ahmad K, Henikoff S. 2014. High-resolution mapping of transcription factor binding sites on native chromatin. *Nat Methods* **11:** 203–209. doi:10.1038/nmeth.2766

Khanna A, Böckelman C, Hemmes A, Junttila MR, Wiksten JP, Lundin M, Junnila S, Murphy DJ, Evan GI, Haglund C, et al. 2009. MYC-dependent regulation and prognostic role of CIP2A in gastric cancer. *J Natl Cancer Inst* **101:** 793–805. doi:10.1093/jnci/djp103

Kretzner L, Blackwood EM, Eisenman RN. 1992. Myc and Max proteins possess distinct transcriptional activities. *Nature* **359:** 426–429. doi:10.1038/359426a0

Kuleshov MV, Jones MR, Rouillard AD, Fernandez NF, Duan Q, Wang Z, Koplev S, Jenkins SL, Jagodnik KM, Lachmann A, et al. 2016. Enrichr: a comprehensive gene set enrichment analysis Web server 2016 update. *Nucleic Acids Res* **44:** W90–W97. doi:10.1093/nar/gkw377

Langdon WY, Harris AW, Cory S, Adams JM. 1986. The c-myc oncogene perturbs B lymphocyte development in Eμ-*myc* transgenic mice. *Cell* **47:** 11–18. doi:10.1016/0092-8674(86)90361-2

Liberzon A, Birger C, Thorvaldsdóttir H, Ghandi M, Mesirov JP, Tamayo P. 2015. The molecular signatures database hallmark gene set collection. *Cell Syst* **1:** 417–425. doi:10.1016/j.cels.2015.12.004

Lindeman GJ, Harris AW, Bath ML, Eisenman RN, Adams JM. 1995. Overexpressed max is not oncogenic and attenuates myc-induced lymphoproliferation and lymphomagenesis in transgenic mice. *Oncogene* **10:** 1013–1017.

Liu H, Tang X, Srivastava A, Pécot T, Daniel P, Hemmelgarn B, Reyes S, Fackler N, Bajwa A, Kladney R, et al. 2015. Redeployment of Myc and E2f1-3 drives Rb-deficient cell cycles. *Nat Cell Biol* **17:** 1036–1048. doi:10.1038/ncb3210

Machanick P, Bailey TL. 2011. MEME-ChIP: motif analysis of large DNA datasets. *Bioinformatics* **27:** 1696–1697. doi:10.1093/bioinformatics/btr189

Pérez-Olivares M, Trento A, Rodriguez-Acebes S, González-Acosta D, Fernández-Antorán D, Román-García S, Martinez D, López-Briones T, Torroja C, Carrasco YR, et al. 2018. Functional interplay between c-Myc and Max in B lymphocyte differentiation. *EMBO Rep* **19:** e45770. doi:10.15252/embr.201845770

Popov N, Schülein C, Jaenicke LA, Eilers M. 2010. Ubiquitylation of the amino terminus of Myc by $SCF^{\beta\text{-}TrCP}$ antagonizes SCF^{Fbw7}-mediated turnover. *Nat Cell Biol* **12:** 973–981. doi:10.1038/ncb2104

Ren Y, Bi C, Zhao X, Lwin T, Wang C, Yuan J, Silva AS, Shah BD, Fang B, Li T, et al. 2018. PLK1 stabilizes a MYC-dependent kinase network in aggressive B cell lymphomas. *J Clin Invest* **128:** 5517–5530. doi:10.1172/JCI122533

Romero OA, Torres-Diz M, Pros E, Savola S, Gomez A, Moran S, Saez C, Iwakawa R, Villanueva A, Montuenga LM, et al. 2014. MAX inactivation in small cell lung cancer disrupts MYC-SWI/SNF programs and is synthetic lethal with BRG1. *Cancer Discov* **4:** 292–303. doi:10.1158/2159-8290.CD-13-0799

Sabò A, Kress TR, Pelizzola M, de Pretis S, Gorski MM, Tesi A, Morelli MJ, Bora P, Doni M, Verrecchia A, et al. 2014. Selective transcriptional regulation by Myc in cellular growth

control and lymphomagenesis. *Nature* **511:** 488–492. doi:10.1038/nature13537

Schaefer IM, Wang Y, Liang CW, Bahri N, Quattrone A, Doyle L, Mariño-Enriquez A, Lauria A, Zhu M, Debiec-Rychter M, et al. 2017. MAX inactivation is an early event in GIST development that regulates p16 and cell proliferation. *Nat Commun* **8:** 14674. doi:10.1038/ncomms14674

Schuhmacher M, Kohlhuber F, Holzel M, Kaiser C, Burtscher H, Jarsch M, Bornkamm GW, Laux G, Polack A, Weidle UH, et al. 2001. The transcriptional program of a human B cell line in response to Myc. *Nucleic Acids Res* **29:** 397–406. doi:10.1093/nar/29.2.397

Shen L, Shao N, Liu X, Nestler E. 2014. ngs.plot: quick mining and visualization of next-generation sequencing data by integrating genomic databases. *BMC Genomics* **15:** 284. doi:10.1186/1471-2164-15-284

Shen-Li H, O'Hagan RC, Hou H Jr, Horner JW II, Lee HW, DePinho RA. 2000. Essential role for Max in early embryonic growth and development. *Genes Dev* **14:** 17–22.

Skene PJ, Henikoff S. 2017. An efficient targeted nuclease strategy for high-resolution mapping of DNA binding sites. *Elife* **6:** e21586. doi:10.7554/eLife.21856

Steiger D, Furrer M, Schwinkendorf D, Gallant P. 2008. Max-independent functions of Myc in *Drosophila* melanogaster. *Nat Genet* **40:** 1084–1091. doi:10.1038/ng.178

Struntz NB, Chen A, Deutzmann A, Wilson RM, Stefan E, Evans HL, Ramirez MA, Liang T, Caballero F, Wildschut MHE, et al. 2019. Stabilization of the Max homodimer with a small molecule attenuates Myc-driven transcription. *Cell Chem Biol* **26:** 711–723.e14. doi:10.1016/j.chembiol.2019.02.009

Subramanian A, Tamayo P, Mootha VK, Mukherjee S, Ebert BL, Gillette MA, Paulovich A, Pomeroy SL, Golub TR, Lander ES, et al. 2005. Gene set enrichment analysis: a knowledge-based approach for interpreting genome-wide expression profiles. *Proc Natl Acad Sci* **102:** 15545–15550. doi:10.1073/pnas.0506580102

Vallespinós M, Fernández D, Rodríguez L, Alvaro-Blanco J, Baena E, Ortiz M, Dukovska D, Martínez D, Rojas A, Campanero MR, et al. 2011. B Lymphocyte commitment program is driven by the proto-oncogene *c-Myc*. *J Immunol* **186:** 6726–6736. doi:10.4049/jimmunol.1002753

Welcker M, Orian A, Jin J, Grim JE, Harper JW, Eisenman RN, Clurman BE. 2004. The Fbw7 tumor suppressor regulates glycogen synthase kinase 3 phosphorylation-dependent c-Myc protein degradation. *Proc Natl Acad Sci* **101:** 9085–9090. doi:10.1073/pnas.0402770101

Wiegering A, Pfann C, Uthe FW, Otto C, Rycak L, Mäder U, Gasser M, Waaga-Gasser AM, Eilers M, Germer CT. 2013. CIP2A influences survival in colon cancer and is critical for maintaining Myc expression. *PLoS One* **8:** e75292. doi:10.1371/journal.pone.0075292

Yada M, Hatakeyama S, Kamura T, Nishiyama M, Tsunematsu R, Imaki H, Ishida N, Okumura F, Nakayama K, Nakayama KI. 2004. Phosphorylation-dependent degradation of c-Myc is mediated by the F-box protein Fbw7. *EMBO J* **23:** 2116–2125. doi:10.1038/sj.emboj.7600217

Yin X, Giap C, Lazo JS, Prochownik EV. 2003. Low molecular weight inhibitors of Myc–MAX interaction and function. *Oncogene* **22:** 6151–6159. doi:10.1038/sj.onc.1206641

Zirath H, Frenzel A, Oliynyk G, Segerstrom L, Westermark UK, Larsson K, Munksgaard Persson M, Hultenby K, Lehtio J, Einvik C, et al. 2013. MYC inhibition induces metabolic changes leading to accumulation of lipid droplets in tumor cells. *Proc Natl Acad Sci* **110:** 10258–10263. doi:10.1073/pnas.1222404110